1883-1893.
Meister, S. M., & Kent, S. B. H. (1984) in *Peptides: Structure and Function* (Hruby, V. J., Ed.) pp 99-102, Pierce Chemical Co., Rockford, IL.
Merrifield, R. B. (1963) *J. Am. Chem. Soc. 85*, 2149-2154.
Moser, B., Clark-Lewis, I., Zwahlen, R., & Baggiolini, M. (1990) *J. Exp. Med. 171*, 1797-1802.
Oschkinat, H., Gresinger, C., Kraulis, P. J., Sorensen, O. W., Ernst, R. R., Gronenborn, A. M., & Clore, G. M. (1989) *Nature 322*, 374-376.
Peveri, P., Walz, A., Dewald, B., & Baggiolini, M. (1988) *J. Exp. Med. 167*, 1547-1559.
Richmond, A., Balentien, E., Thomas, H. G., Flaggs, G., Barton, E., Spiess, J., Bordoni, R., Francke, V., & Derynck, R. (1988) *EMBO J. 7*, 2025-2033.
Sarin, V. K., Kent, S. B. H., Tam, J. P., & Merrifield, R. B. (1981) *Anal. Biochem. 117*, 147-157.
Schiffmann, N. E., Corcoran, B. A., & Wahl, S. M. (1975) *Proc. Natl. Acad. Sci. U.S.A. 72*, 1059-1062.
Schneider, J., & Kent, S. B. H. (1988) *Cell 54*, 363-368.
Schroder, J. M., & Christophers, E. (1989) *J. Immunol. 142*, 244-251.
Schroder, J. M., Mrowietz, V., Morita, E., & Christophers, E. (1987) *J. Immunol. 139*, 3474-3483.
Tam, J. P., Heath, W. F., & Merrifield, R. B. (1983) *J. Am. Chem. Soc. 105*, 6442-6455.
Tanaka, S., Robinson, E. A., Yoshimura, T., Matsushima, K., Leonard, E. J., & Appella, E. (1988) *FEBS Lett. 236*, 467-470.
Van Damme, J., Van Beeumen, J., Opdenakker, G., & Billiau, A. (1988) *J. Exp. Med. 167*, 1364-1376.
Walz, A., & Baggiolini, M. (1989) *Biochem. Biophys. Res. Commun. 159*, 969-975.
Walz, A., & Baggiolini, M. (1990) *J. Exp. Med. 171*, 449-454.
Walz, A., Peveri, P., Aschauer, H., & Baggiolini, M. (1987) *Biochem. Biophys. Res. Commun. 149*, 755-761.
Walz, A., Dewald, B., von Tscharner, V., & Baggiolini, M. (1989) *J. Exp. Med. 170*, 1745-1750.
Westwick, J., Li, S. W., & Camp, R. D. (1989) *Immunol. Today 10*, 146-147.
Wlodawer, A., Miller, M., Jaskolski, M., Sathyanarayana, B. K., Baldwin, E., Weber, I. T., Selk, L. M., Clawson, L., Schneider, J., & Kent, S. B. H. (1989) *Science 245*, 616-621.
Woo, D. D. L., Clark-Lewis, I., Chait, B. T., & Kent, S. B. H. (1989) *Protein Eng. 3*, 29-37.
Yoshimura, T., Matsushima, K., Oppenheim, J. J., & Leonard, E. J. (1987a) *J. Immunol. 139*, 788-793.
Yoshimura, T., Matsushima, K., Tanaka, S., Robinson, E. A., Appella, E., Oppenheim, J. J., & Leonard, E. J. (1987b) *Proc. Natl. Acad. Sci. U.S.A. 84*, 9233-9237.

Porcine Pancreatic Phospholipase A_2: Sequence-Specific ^1H and ^{15}N NMR Assignments and Secondary Structure†

Niek Dekker,‡ Anton R. Peters,§ Arend J. Slotboom,‡ Rolf Boelens,§ Robert Kaptein,*,§ and Gerard de Haas‡

Center for Biomembranes and Lipid Enzymology and Bijvoet Center for Biomolecular Research, State University of Utrecht, P.O. Box 80.054, 3584 CH Utrecht, The Netherlands

Received September 18, 1990

ABSTRACT: The solution structure of porcine pancreatic phospholipase A_2 (124 residues, 14 kDa) has been studied by two-dimensional homonuclear ^1H and two- and three-dimensional heteronuclear ^{15}N-^1H nuclear magnetic resonance spectroscopy. Backbone assignments were made for 117 of the 124 amino acids. Short-range nuclear Overhauser effect (NOE) data show three α-helices from residues 1-13, 40-58, and 90-109, an antiparallel β-sheet for residues 74-85, and a small antiparallel β-sheet between residues 25-26 and 115-116. A ^{15}N-^1H heteronuclear multiple-quantum correlation experiment was used to monitor amide proton exchange over a period of 22 h. In total, 61 amide protons showed slow or intermediate exchange, 46 of which are located in the three large helices. Helix 90-109 was found to be considerably more stable than the other helices. For the β-sheets, four hydrogen bonds could be identified. The secondary structure of porcine PLA in solution, as deduced from NMR, is basically the same as the structure of porcine PLA in the crystalline state. Differences were found in the following regions, however. Residues 1-6 in the first α-helix are less structured in solution than in the crystal structure. Whereas in the crystal structure residues 24-29 are involved both in a β-sheet with residues 115-117 and in a hairpin turn, the expected hydrogen bonds between residues 24-117 and 25-29 do not show slow exchange behavior. This and the absence of several expected NOEs implie that this region has a less well defined structure in solution. Finally, the hydrogen bond between residues 78-81, which is part of a β-sheet, does not show slow exchange behavior.

Phospholipase A_2 (PLA[1], EC 3.1.1.4) is a calcium-dependent enzyme that specifically cleaves the 2-acyl linkage of *sn*-3-phosphoglycerides (Waite, 1987). Phospholipases occur both extra- and intracellularly. The extracellular PLA's from mammalian pancreas and from snake venom (Waite, 1987;

† The investigations were carried out under the auspices of the Netherlands Organization for Chemical Research (SON) with financial support from the Netherlands Organization for Scientific Research (NWO).
* Address correspondence to this author.
‡ Center for Biomembranes and Lipid Enzymology.
§ Bijvoet Center for Biomolecular Research.

[1] Abbreviations: PLA, phospholipase A_2; NMR, nuclear magnetic resonance; COSY, correlated spectroscopy; NOE, nuclear Overhauser enhancement; NOESY, nuclear Overhauser enhancement spectroscopy; TOCSY, total correlation spectroscopy; HOHAHA, homonuclear Hartmann-Hahn; HMQC, heteronuclear multiple-quantum correlation spectroscopy; 2D, two dimensional; ppm, parts per million; TPPI, time-proportional phase increment; SCUBA, stimulated cross-peaks under bleached α's; TMS, tetramethylsilane.

0006-2960/91/0430-3135$02.50/0

Volwerk & de Haas, 1982) and also the mammalian intracellular PLA's (Forst et al., 1986; Hayakawa et al., 1988; Ono et al., 1988) exhibit a high degree of sequence homology. Phospholipases are characterized by a low molecular mass (14 kDa), six to seven disulfide bridges, and a high stability against strong acids, heat, and detergents. The X-ray structures of the enzymes from porcine and bovine pancreas, and from the venom of the rattlesnake *Crotalus atrox*, have been determined (Dijkstra et al., 1981, 1983; Brunie et al., 1985), and a mechanism of catalysis has been proposed (Verheij et al., 1980). PLA is an enzyme that is activated in the presence of aggregated substrate (Waite, 1987). Two kinds of models have been proposed to explain this interfacial activation process, which is common to all lipolytic enzymes. The substrate models are based on a restricted conformation of the substrate molecules in the lipid–water interface, which is the optimal configuration to fit in the active center of PLA and to be hydrolyzed. The enzyme models support a conformational change of the enzyme upon binding to a lipid–water interface that leads to an optimalization of the active center geometry. Until now the enzyme structure has only been studied in detail by X-ray crystallography. Although much of our current understanding derives from these studies, the X-ray method is less suited to the study of the interaction of the enzyme with aggregated substrate analogues. Our aim is to use high-resolution NMR spectroscopy to study the protein's structure and dynamics. This technique has the advantage that, once the NMR signals have been assigned, the interaction of the protein with inhibitors and substrate analogues under micellar conditions and the changes of the protein's structure upon micelle binding can be studied. There have been a number of earlier NMR studies of the enzyme (Aguiar et al., 1979; Jansen et al., 1978, 1979; Egmond et al., 1980, 1983; Fisher et al., 1989), but as yet only a limited number of resonance assignments have been made, greatly limiting the information that one can obtain from NMR experiments. Thus far, 3D structure determinations by NMR have been limited to relatively small proteins. This size limitation is due to spectral crowding, short T_2 relaxation times, and increasing line widths for proteins containing more than about 100 residues. Recently, the use of heteronuclear 3D NMR spectroscopy has been proposed for facilitating the simplification of NMR spectra of larger systems (Zuiderweg & Fesik, 1989; Marion et al., 1989a). The 3D experiment is a combination of homonuclear 2D NOE [for a review, see Jeener et al. (1979)] and heteronuclear multiple-quantum correlation (HMQC) spectroscopy (Müller, 1979), which provides a method for unambiguous identification of through-space nuclear Overhauser connectivities.

Here we describe the sequential assignment of PLA. To this end, we used conventional 2D NMR techniques like 2D NOE and 2D TOCSY [for a review, see Bax (1989)] in combination with the 3D NOESY-HMQC and 3D TOCSY-HMQC experiments. For the heteronuclear experiments we have used uniform ^{15}N labeling. We have also made use of the incorporation of ^{15}N-labeled amino acids to obtain specific resonance assignments.

Materials and Methods

Sample Preparation. Porcine pancreatic PLA was prepared from pancreas by following standard procedures previously described (Nieuwenhuizen et al., 1974). PLA was biosynthetically ^{15}N-labeled by using an efficient *Escherichia coli* plasmid expression system (de Geus et al., 1987). The MC4100 *E. coli* were grown in minimal medium with $^{15}NH_4Cl$ (Cambridge Isotopes Laboratory) as the sole nitrogen source. The purification from *E. coli* was done as previously described (de Geus et al., 1987). Specific labeling with [^{15}N]glycine was achieved by using the PC1552 strain (Phabagen collection, Utrecht, The Netherlands) of *E. coli*, which is auxotrophic for that amino acid, with a concentration of 100 mg of [^{15}N]Gly/10 L of minimal medium. In this way 3 mg of pure [^{15}N]Gly-PLA was obtained. For the incorporation of [^{15}N]leucine, 0.5 g of the labeled amino acid was added prior to induction of a 10-L minimal medium culture of MC4100 *E. coli*. [^{15}N]Gly and [^{15}N]Leu were purchased from Sigma.

The NMR samples were typically 1.5 mM enzyme in either 99.96% D_2O or 95% H_2O/5% D_2O, containing 50 mM $CaCl_2$ and 150 mM NaCl. The samples enriched with ^{15}N were recorded in H_2O containing the same salts. The pH (uncorrected meter reading) was adjusted to 4.3 by the addition of microliter quantities of 0.1 M solutions of DCl and NaOD. For the experiments in D_2O all exchangeable protons were replaced by deuterons. To this end, the enzyme was dissolved in 99.96% D_2O at acidic pH and heated to 80 °C for 10 min, followed by repeated lyophilization and dissolution in D_2O. In the 3D NOESY-HMQC and 3D TOCSY-HMQC experiments, a 4 mM protein concentration was used. Although at this high protein concentration aggregation of the protein gives rise to line broadening, sensitivity increases considerably.

NMR Spectroscopy. Two-dimensional NMR spectra were recorded on a Bruker AM 500 or Bruker AM 600 spectrometer (the latter at the SON hf-NMR facility, Nijmegen University, The Netherlands). Both spectrometers were interfaced with an Aspect 3000 computer. The data were processed on DEC Vaxstations with the "Triton" software library (written in FORTRAN 77). All two-dimensional spectra were recorded in the pure-phase absorption mode by application of TPPI (Marion & Wüthrich, 1983). The HDO signal was suppressed by presaturation during the recycle delay and during the mixing time of the NOESY experiments. The recording temperatures were in the range 38–40 °C. For ^1H nuclei, ppm values were calibrated by using the resonance position of the water line, with a chemical shift of 4.60 ppm relative to TMS; for ^{15}N nuclei, a value of 22.3 ppm for NH_4^+ relative to liquid NH_3 was used.

The 2D TOCSY spectra (Braunschweiler et al., 1983; Davis & Bax, 1985a) at 500 MHz were recorded with a MLEV-17 mixing sequence (Bax & Davis, 1985) with total mixing times of 21–55 ms. A clean-TOCSY spectrum at 500 MHz was obtained in H_2O to yield relayed NH–C_βH cross-peaks (Griesinger, 1988). The 2D NOE spectra were recorded with a 32-step phase cycle (States et al., 1982) with a mixing time of 150 ms for the D_2O spectrum and mixing times of 50, 100, 150, and 200 ms for the H_2O spectra. The cross-peaks around 4.6 ppm, which are normally irradiated together with the water line, were made observable by using the SCUBA method (Brown et al., 1988). The decoupler was switched off prior to the start of the 2D experiment. The cross-relaxation delay (set to 70 ms) and the NOE mixing time were interrupted in the middle by a composite 180° pulse.

Typically a data set of 400 × 2K was obtained, which was processed with a sine-bell window shifted over $\pi/6$ or $\pi/4$ in ω_2 and $\pi/3$ in ω_1. Zero-filling was used to obtain a spectral data matrix of 1K × 1K. Fourth-order polynomial base-line corrections in each domain were applied after the double Fourier transformation was completed (Boelens et al., 1985). For spectra recorded in H_2O separate base-line corrections in ω_2 on the left- and right-hand side of the H_2O line were carried out.

The heterocorrelation experiments were recorded by using a 5-mm ^1H broad-band inverse detection probe at 500 MHz.

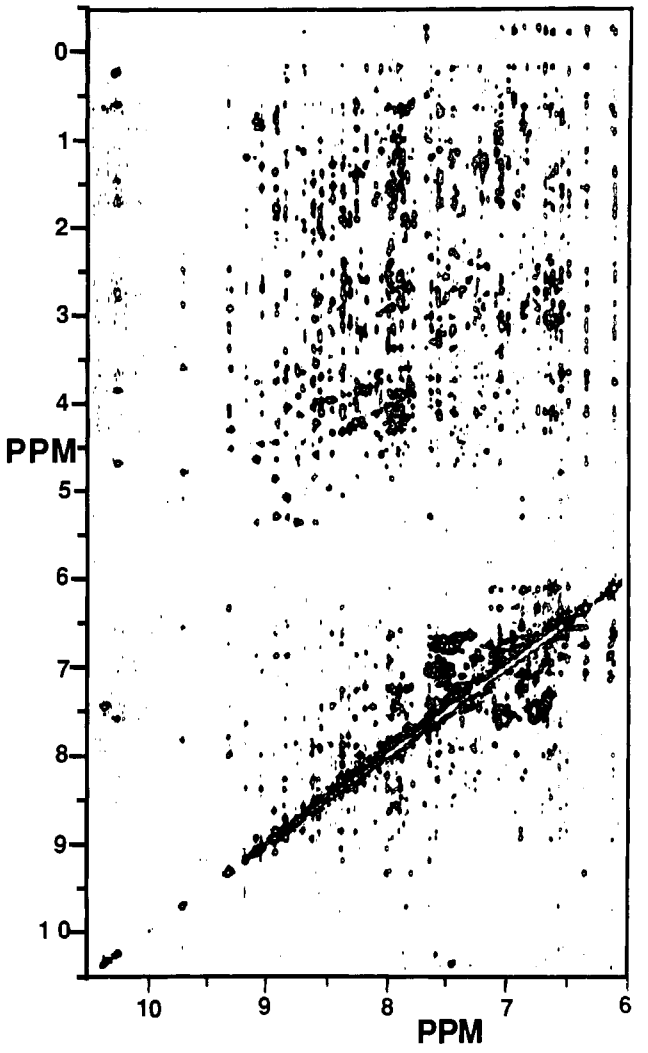

FIGURE 1: 600-MHz 2D NOE spectrum of 1.5 mM porcine PLA in H_2O solution with a mixing time of 200 ms.

Heteronuclear decoupling was achieved by a Bruker BSV-3 X-nucleus broad-band decoupler with GARP decoupling (Shaka et al., 1985). Solvent suppression was carried out during the 1-s relaxation delay by using a DANTE pulse sequence (94-μs delay, 6-μs pulse, low power) (Jeener et al., 1979). Other ^1H pulses were delivered from the same ^1H-decoupler amplifier. The heteronuclear J-coupling refocusing time was set to 4 ms. A homospoil pulse was applied in the middle of the mixing time (set to 100 ms) to minimize coherent transfer of magnetization between scalar-coupled spins (Jeener et al., 1979). For the 2D HMQC experiment (Müller, 1979) the proton carrier was set on the H_2O resonance and the ^{15}N carrier in the center of the ^{15}N spectrum at 108.9 ppm, between the amide backbone resonances and the side-chain arginine resonances. A spectral width of 56.0 ppm was used in ω_1 and 14.70 ppm was used in ω_2. The arginine side-chain NH_2 resonances, which do not give any NOEs, were folded back between the arginine ϵ-amine and backbone amide resonances. The 3D NOESY-HMQC experiment was recorded by using a pulse sequence similar to the one used by Marion et al. (1989a). For the 3D TOCSY-HMQC experiment, HOHAHA mixing was achieved by the use of the trim-pulse/60°-pulse/300°-pulse sequence (Davis & Bax, 1985b). The resulting data sets consisted of 200 × 128 × 1024 points (t_1, t_2, t_3 = ^1H, ^{15}N, ^1H). The data were processed with a sine-bell shifted over $\pi/3$ in all dimensions and with zero-filling. Only the low-field region of the ω_3 data set was

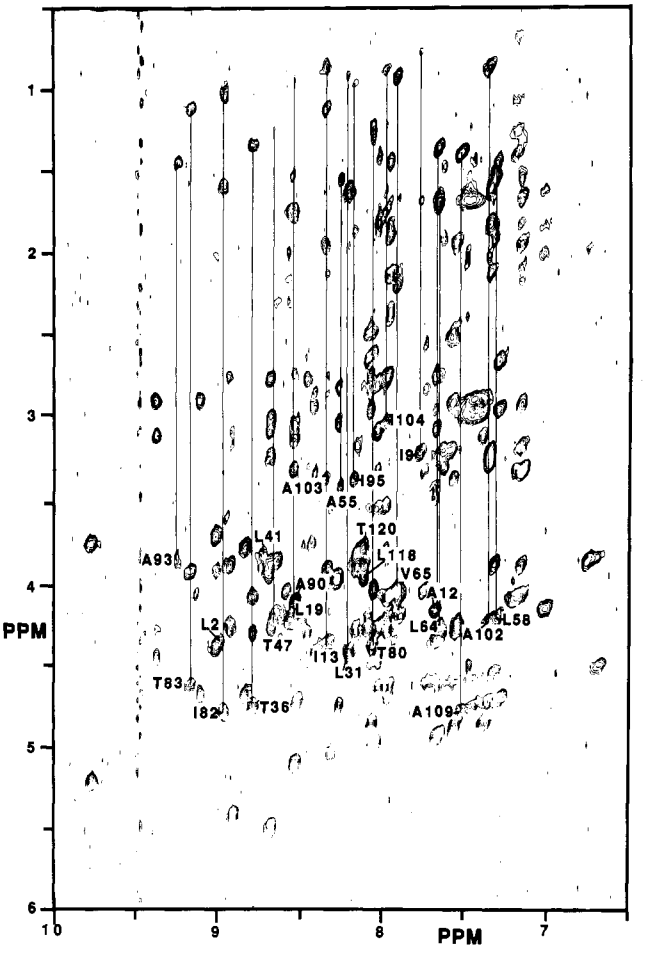

FIGURE 2: 500-MHz 2D TOCSY spectrum of 1.5 mM PLA in H_2O with a mixing time of 49 ms. For the aliphatic residues Leu, Ala, Val, Thr, and Ile, relay connectivities are indicated.

transformed in t_1 and t_2 for a total data set size of 512 × 128 × 450 points (ω_1, ω_2, ω_3).

Results and Discussion

Figure 1 depicts a portion of a 2D NOE spectrum of porcine pancreatic PLA in H_2O. Around 8 ppm a large number of overlapping amide signals are present. The corresponding clean-TOCSY spectrum is shown in Figure 2. For a number of resonances relay connectivities could be assigned. Also in this spectrum the NH–C_αH fingerprint region shows overlap for the amide protons around 8 ppm.

Assignment Strategy. The 2D TOCSY and 2D COSY spectra of PLA in D_2O show regions of heavy overlap in the aliphatic region. The standard method for sequential assignment proposed by Wüthrich (1986), in which spin system identification is the starting point, is difficult to apply to PLA. This could be accomplished only for a limited number of residues. For PLA the assignment was done by starting with sequential identification of secondary structure (Englander & Wand, 1987). This resulted in stretches of residues linked by NH–NH or C_αH–NH NOE connectivities based on the 2D NOE (Figure 1) and 2D TOCSY (Figure 2) spectra in H_2O. These assignments were transferred from the 2D NOE spectra to the 2D TOCSY and 2D COSY spectra in D_2O for confirmation and extension of the side-chain identification. The 3D NOESY-HMQC and 3D TOCSY-HMQC experiments were used to confirm these assignments and to extend the procedure in regions of overlap.

Identification of the ^1H Spin Systems of Ala, Thr, Val, and

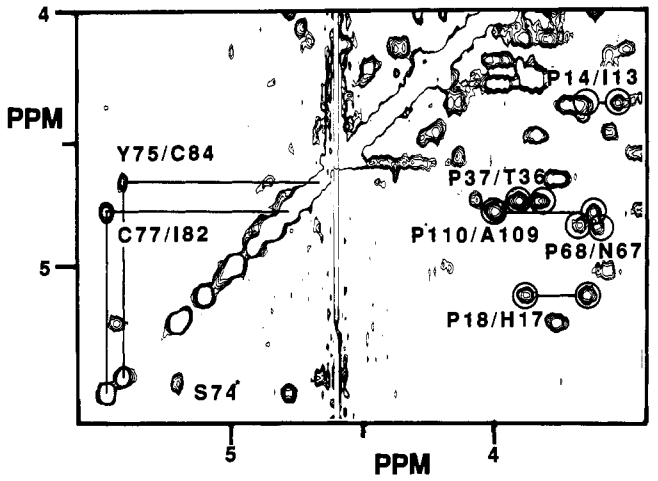

FIGURE 3: Aliphatic part of the 500-MHz 2D NOE spectrum of 1.5 mM PLA, pH 4.3, in D_2O recorded with a mixing time of 150 ms. The sequential $C_\alpha H$–$C_{\delta\delta'}H$ cross-peaks for the X–Pro sequences in PLA are indicated with circles. Indicated are the $C_\alpha H$–$C_\alpha H$ contacts in the β-sheet between Tyr75–Cys84 and Cys77–Ile82. The star indicates the exchange cross-peak between the two C_α proton resonance positions of Ser74 (see text).

Gly. PLA contains eight alanines, six threonines, two valines, and six glycines. All eight alanines could be identified by their $C_\alpha H$–$C_\beta H$ cross-peak in the aliphatic region of the 2D TOCSY spectrum in D_2O with a short mixing time. The threonine relay cross-peak $C_\alpha H$–$C_\gamma H$ is absent at short mixing times but shows up when longer mixing times are used. With this discrimination, four threonines could be identified. The valines have a unique spin system and could be identified on the basis of $C_\alpha H$–$C_\beta H$ cross-peaks, $C_\beta H$–C_γ methyl cross-peaks, and the presence of a $C_\alpha H$–C_γ methyl cross-peak in the TOCSY spectrum with a long mixing time. One of the valines, identified as Val65 in a later stage, has methyl groups that have degenerate chemical shifts and thus shows only a single relayed cross-peak. In the 2D TOCSY spectrum recorded in H_2O, the assignments could be extended to the corresponding amide position for the alanines, the valines, and the four threonines (Figure 2), except for the N-terminal Ala1. The amide proton of Val38 has a downfield shift of 10.29 ppm; for this valine only a NH–$C_\alpha H$ cross-peak could be assigned because of its unfavorable position relative to the carrier frequency. For the assignment of the glycine residues, labeling with [^{15}N]Gly was used.

Aromatic Spin Systems. The connectivity patterns of the aromatic ring spin systems (Wüthrich, 1986) have been previously assigned in a sequence-specific way on the basis of the crystal structure (Fisher et al., 1989). These assignments were extended to the backbone part of these residues on the basis of the intraresidual NH–ortho ring proton NOE, resulting in AMX spin systems that could be used in the sequential assignment procedure as starting points.

Identification of X–Pro Sequences. In Figure 3 all the sequential $C_\alpha H$–$C_{\delta\delta'}H$ connectivities for the proline residues are indicated. The identification of the spin systems for the proline residues, starting from the $C_{\delta\delta'}$ protons, was hampered due to weak or absent correlations to the $C_{\gamma\gamma'}$ protons in the 2D TOCSY spectra.

Identification of Amino Acid Type Using Specific Labeling. With residue type specific labeling procedures a number of starting points for the sequential assignment were obtained. The 2D HMQC spectrum of a 0.5 mM sample of the [^{15}N]glycine-labeled enzyme gives rise to six cross-peaks for all glycines present in PLA (Figure 4). The ^{15}N chemical

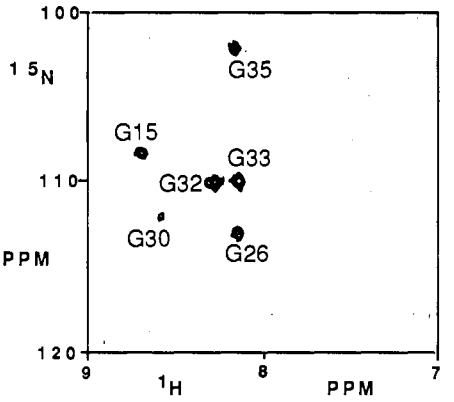

FIGURE 4: 500-MHz ^{15}N–^{1}H HMQC spectrum of 0.5 mM [^{15}N]-glycine-labeled PLA in H_2O. Cross-peaks for all six glycines in PLA are present and sequentially assigned.

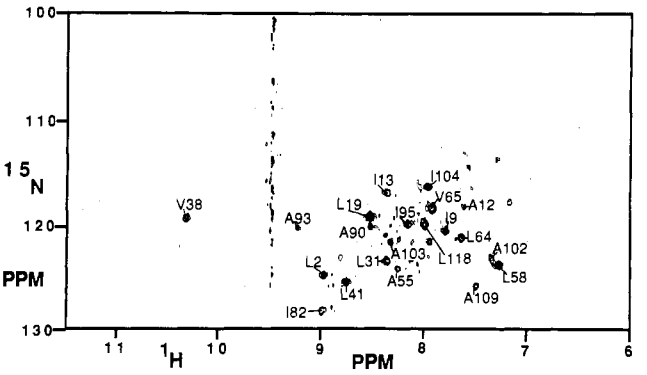

FIGURE 5: 500-MHz ^{15}N–^{1}H HMQC spectrum of 1.5 mM [^{15}N]-leucine-labeled PLA in H_2O. Note the cross labeling into valine and isoleucine and the cross labeling from valine into alanine.

shift for the glycines was found to be at high field with respect to the other amide resonances. In the 2D NOE and 2D TOCSY spectra in H_2O the corresponding resonances of the C_α protons could be assigned. It turned out that three glycines have equivalent C_α protons. For the three other glycine spin systems the off-diagonal $C_\alpha H$–$C_{\alpha'}H$ cross-peaks were observed in the 2D TOCSY spectrum in D_2O.

Labeling with [^{15}N]leucine yielded a 2D HMQC spectrum with 21 cross-peaks (Figure 5) of which the 7 most intense cross-peaks were leucines. Strong scrambling of the amine label occurred due to transaminase activity. The biosynthesis of leucine, isoleucine, and valine is strongly interrelated; therefore labeling also occurred for isoleucine and valine. Both valines and all five isoleucines could be identified. Transamination of the amino group of valine to alanine is known to be a minor pathway for the biosynthesis of alanine. In the 2D HMQC spectrum it was found that strong cross labeling occurred for valine, and these relatively high amounts of labeled valine resulted in labeling of alanine. Seven cross-peaks could be assigned to alanine residues. In PLA eight alanines are present, but the N-terminal Ala1 gives no cross-peak.

^{15}N–^{1}H 2D HMQC. In the 2D HMQC spectrum of fully ^{15}N-enriched PLA, 147 cross-peaks are present (Figure 6). On the basis of the amino acid composition one expects 118 backbone amide correlations, 14 pairs of side-chain amide correlations for asparagine and glutamine, and one indole correlation for Trp3. The α-amino group of Ala1, the histidine side-chain imino protons, and the lysine side-chain amino protons exchange too rapidly with the solvent and therefore are not observable. Upfield of the amide region are four cross-peaks for the ϵN proton of the arginines, together with

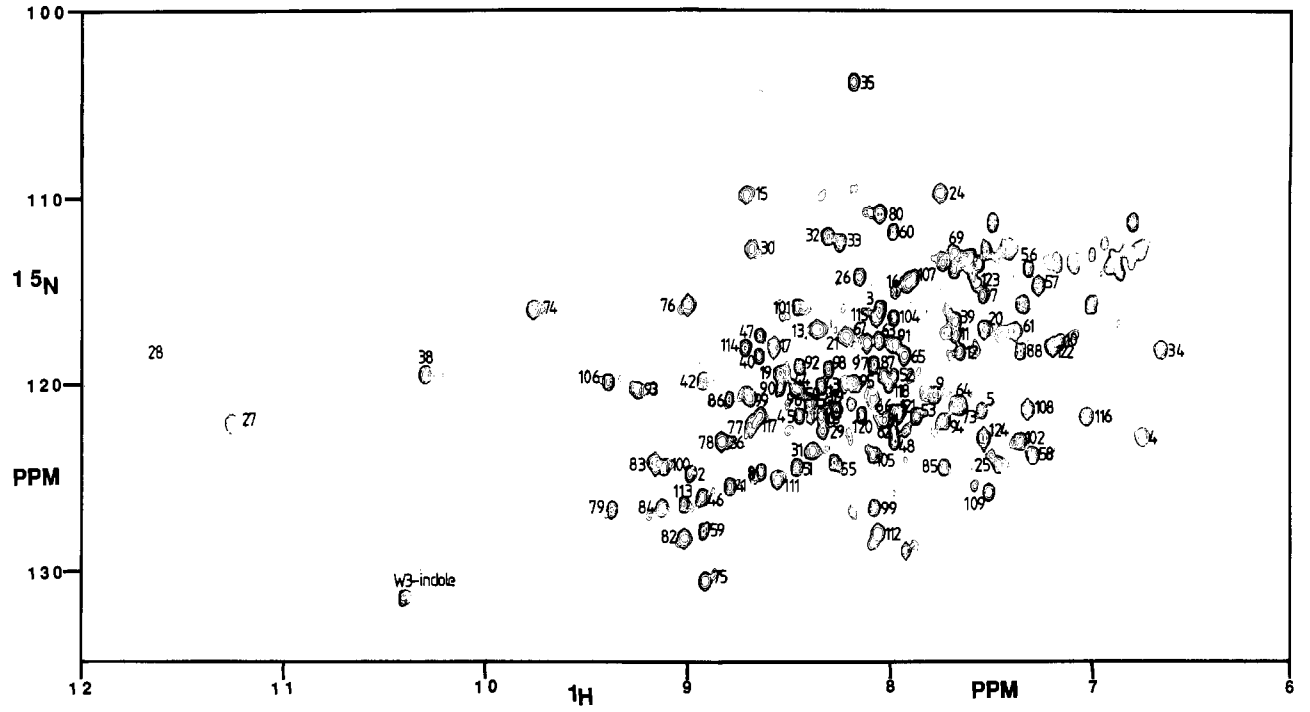

FIGURE 6: 500-MHz ^{15}N-^{1}H HMQC spectrum of 1.5 mM ^{15}N-labeled PLA in H_2O, pH 4.3 at 313 K. There are 111 cross-peaks assigned to specific residues in PLA.

a broad cross-peak of the ηN protons of these residues. The indole proton of Trp3 was assigned on the basis of its TOCSY correlation to its H2 ring proton. The correlation between ^{1}H and ^{15}N chemical shifts is not strong, giving rise to an improved resolution, which was used in the 3D NOESY-HMQC experiment.

3D Heteronuclear Experiments. In the early stage of the assignment procedure only the 2D homonuclear NMR spectra were available. With the homonuclear technique, around 40% of the backbone protons could be assigned. Many of the sequential NH–NH contacts in the 7.5–6.5 ppm region remained unassigned due to overlap with the aromatic and amine protons. With the labeling techniques the assignment could be almost completed. Figure 7 is a typical example of one of the slices of the 3D experiments. At a ^{15}N chemical shift of 125.4 ppm, 14 amide resonances could be assigned in the 3D NOESY-HMQC experiment (Figure 7A) with their corresponding NOE cross-peaks. In the corresponding 3D TOCSY-HMQC experiment (Figure 7B), 11 intraresidual NH–C_αH cross-peaks could be identified, from which 7 amide protons showed a relay connectivity to their C_βH. In the 3D planes the amide positions are mostly well separated. For example, the Lys108 amide proton at 7.31 ppm is resolved, and the corresponding NOE and TOCSY cross-peaks can be assigned unambiguously (Figure 7), whereas five overlapping resonances are present within 0.05 ppm in the 2D spectra (Figures 1 and 2).

Determination of α-Helical Domains. An α-helix is characterized by a continuous stretch of strong sequential NH–NH NOEs and medium-range $d_{\alpha N}(i, i+3)$ and $d_{\alpha\beta}(i, i+3)$ NOEs. In the spectra of PLA the presence of $d_{\alpha\beta}(i, i+3)$ NOEs was not used in the assignment procedure. The aliphatic region in the 2D NOE spectrum is too crowded to assign these NOEs.

Sequential Assignments. The assignments for various peptide fragments will now be discussed in detail.

α-Helix Ala1–Ile13. The N-terminal helix was assigned on the basis of sequential NH–NH connectivities. In this stretch, labeling confirmed the assignment of Leu2, Ile9, Ala12, and Ile13. The Trp3 indole ring NH and H2 protons both have an NOE to the methyl group of Ala1. We interchanged the assignment published earlier (Fisher et al., 1989) for the indole ring H5 and H6 protons of Trp because of the presence of a H4–H5 cross-peak in the COSY spectrum. For Phe5 the NOE between the amide proton and the ortho ring protons was detected. The assignment of the side-chain protons of Arg6 was done by elimination. The spin systems of all four arginine residues were identified in the planes of the 3D NOESY-HMQC spectrum, containing the N_ϵH resonances of the ^{15}N-labeled protein. The assignments of the backbone proton resonances of Arg6 are still uncertain. For residues Gln4 and Phe5 the NH–NH contacts and the NOE cross-peaks from the amide to the side-chain protons are very weak (for Phe5 see Figure 7A). Nevertheless, the aromatic protons of Phe5 have strong long-range NOEs to Ile9, Ala102, and Phe106. The assignment of the NH–NH NOE for Cys11–Ala12 was not possible due to overlap of the amide protons. In the 3D NOESY-HMQC experiment the Cys11(C_βH)–Ala12(NH) NOE could be assigned unambiguously as well as the NH–NH connectivities for Lys10–Cys11 and for Ala12–Ile13.

Residues Pro14–Asp21. Pro14 was assigned on the basis of the C_αH–$C_{\delta\delta'}$H NOE to Ile13 (Figure 3). Gly15 was assigned by specific labeling and shows a C_αH–NH connectivity with Pro14. Ser16 and His17 were assigned by using sequential NOEs. Pro18 shows a sequential C_αH–$C_{\delta\delta'}$H NOE from His17 (Figure 3). Leu19 was assigned by selective labeling and was connected to Pro18 and Met20 in a sequential manner by using C_βH–NH and NH–NH connectivities. Asp21 shows NOEs to Met20. The spin system of Asp21 could not be assigned. The following residues, 22–24, are also unassigned.

Residues Tyr25–Cys27. The amide proton of Tyr25 was assigned on the basis of an NH–ortho ring proton NOE and an NOE to the C_α proton. This C_α proton has a C_αH–C_αH contact to Lys116. NOEs were also assigned from the aromatic ring protons of Tyr25 to the side-chain protons of the Lys116 residue. Gly26 was known from the glycine-labeling

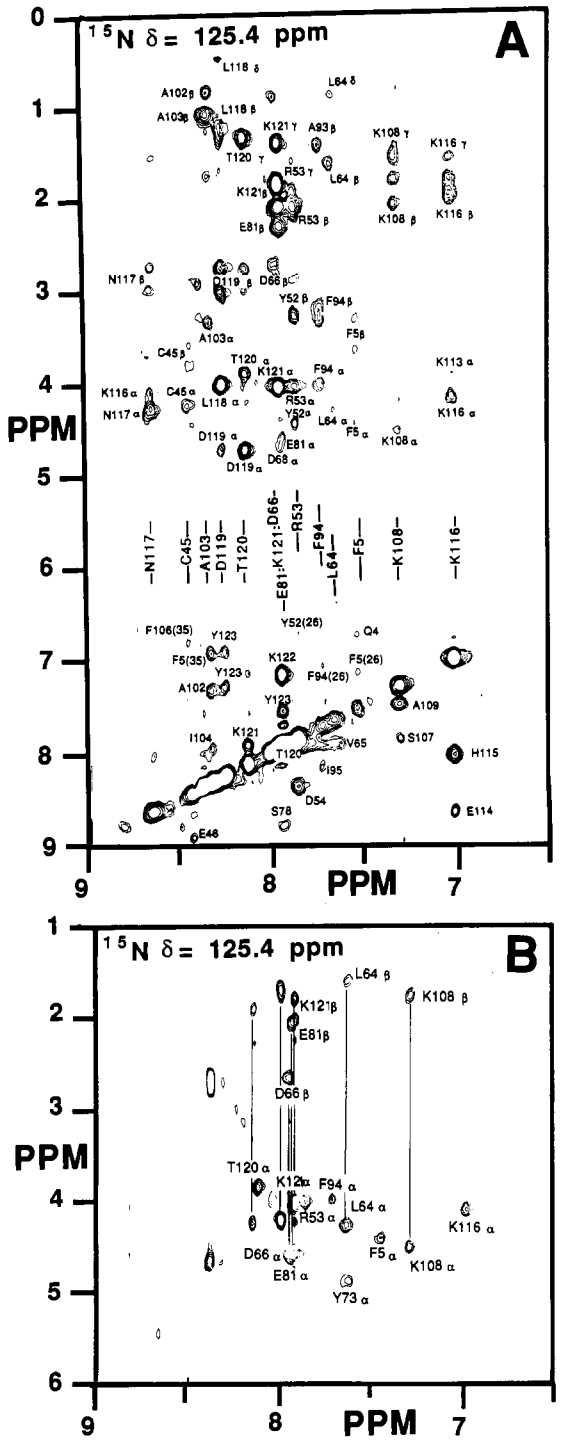

FIGURE 7: Slices of the 500-MHz 3D heteronuclear NMR experiments of 4 mM ^{15}N-labeled PLA in H_2O, pH 4.3 at 313 K. (A) 3D NOESY-HMQC, mixing time of 100 ms. (B) 3D TOCSY-HMQC, spin lock time of 39 ms. The slices shown correspond to a ^{15}N chemical shift δ = 125.4 ppm downfield of liquid ammonia. In this slice the following residues could be identified: Asn117, Cys45, Ala103, Asp119, Thr120, Lys121, Arg53, Phe5, Lys108, and Lys116, whereas in the neighboring planes Tyr73 and Leu64 are present; thus a weak correlation was observed for these residues as well.

experiment, and a sequential C_αH–NH NOE from Tyr25 could be observed. Cys27 could be assigned from sequential C_αH–NH NOEs with Gly26. This amide proton has a chemical shift of 11.21 ppm.

Residues Tyr28–Gly35, the Calcium-Binding Loop. This loop was assigned by using sequential NH–NH and C_αH–NH connectivities. In this part, Gly30, Leu31, Gly32, Gly33, and Gly35 were assigned in the specific-labeling experiments. The amide proton of Tyr28 has an unusual low-field chemical-shift position of 11.70 ppm and shows NH–NH connectivities to Cys27 as well as to Cys29. Also, the NH–ortho ring proton NOE could be identified. This caused us to interchange the assignments of the ortho and meta protons of Tyr28 proposed by Fisher et al. (1989).

Residues Thr36–Asp39. In this sequence Val38 was assigned by specific labeling. Thr36 could be completely assigned in the 2D TOCSY spectrum in H_2O. Sequential assignment was accomplished for the subsequent steps. The sequential C_αH–$C_{\delta\delta'}$H NOEs for Thr36–Pro37 are indicated in Figure 3. A medium-range NOE between the amides of residues 39 and 42 could be identified.

α-Helix Glu40–Leu58. A long stretch of sequential NH–NH and C_βH–NH NOEs could be assigned to this part of the sequence. For the sequential steps from Thr47 to Asp49, the NH–NH cross-peaks could not be unambiguously identified in the 2D NOE spectrum because of overlap of amide protons 47 and 49. The 3D NOESY-HMQC spectrum revealed the correct assignment. For residue type assignments, labeling gave the identification for Leu41, Ala55, and Leu58. Subsequently, the spin systems were completely characterized except for Lys56, which was incompletely assigned.

Residues Asp59–Tyr69. A strong sequential C_αH–NH NOE was found for Leu58–Asp59. The NH–NH NOE for this step is weak, which shows that the preceding helix stops at residue 58. Strong NH–NH NOEs from Asp59 to Ser60 and from Ser60 to Cys61 were found. The sequential assignment could be extended to Tyr69. The assignments of Leu64 and Val65 were confirmed in the labeling experiment. The sequential C_αH–$C_{\delta\delta'}$H NOEs for Asn67–Pro68 were clearly visible as shown in Figure 3. For Tyr69 the NH–ortho ring proton NOE could be detected. Residues 70–72 remain unassigned.

β-Sheet Tyr73–Asn85. The 2D NOE spectrum of PLA reveals two strong C_αH–C_αH contacts in the low-field region of the aliphatic part of the spectrum (Figure 3). This combined with strong sequential C_αH–NH and weak intraresidual NH–C_αH connectivities in the 2D NOE spectrum in H_2O is evident for a β-sheet structure. One of these C_αH–C_αH contacts involves a C_αH at 5.41 ppm belonging to Tyr75 (previously assigned; Fisher et al., 1989) and has NOEs to the aromatic ortho ring protons. In the 2D TOCSY spectra the NH and $C_{\beta\beta'}$ protons of Tyr75 were also assigned. This amide proton has a strong sequential NOE connectivity to the C_αH of Ser74. The amide proton of Ser74 was assigned in the 2D TOCSY spectrum in which the whole spin system is present on the NH line, which occurs at a unique downfield position at 9.72 ppm. This amide proton displays an NOE connectivity to the C_αH of Tyr73. The aromatic ortho ring protons of Tyr73 have NOEs to its C_α and $C_{\beta\beta'}$ protons. The assignment in this strand was extended to Asn79 on the basis of strong sequential C_αH–NH NOEs combined with the information on intraresidual NH–C_αH and NH–$C_{\beta\beta'}$H connectivities from the 2D TOCSY spectrum. From this strand of the β-sheet several NOE connectivities to the other strand were identified; among these there are C_αH–C_αH contacts for Tyr75–Cys84 and Cys77–Ile82 and a NH–NH contact for Ser76–Thr83. The other strand of this antiparallel β-sheet involves residues Glu81–Asn85. In this part the spin systems of Ile82 and Thr83 were assigned in the early stage of the assignment procedure. Strong sequential C_αH–NH connectivities were observed for these residues. Thr80 is present in the loop formed in the β-sheet and was assigned on the basis of sequential NH–NH NOEs to Asn79 and Glu81 in a 2D HMQC-NOE experiment

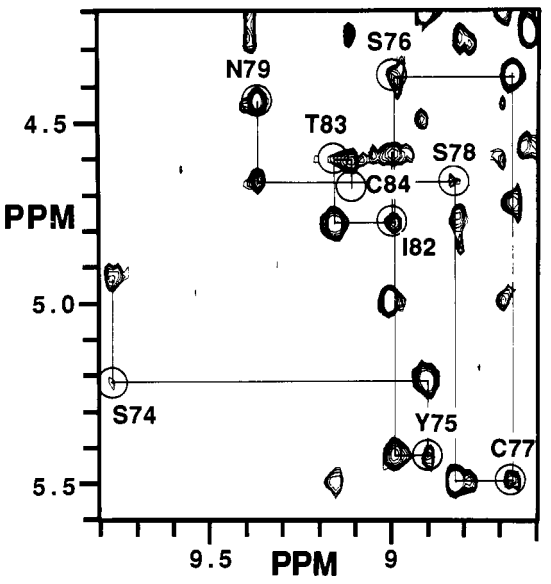

FIGURE 8: Portion of the 600-MHz 2D NOE spectrum of PLA in H_2O solution (mixing time 200 ms), showing the sequential $C_\alpha H$–NH connectivities of the antiparallel β-sheet involving residues Ser74–Asn85. The corresponding TOCSY cross-peaks are circled.

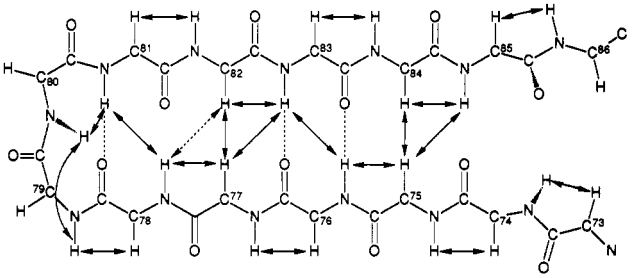

FIGURE 9: NMR analysis of the antiparallel β-sheet. The observed NOE connectivities are indicated by arrows; the dashed arrow indicates a weak NOE. Dashed lines indicate interstrand hydrogen bonds.

(Gronenborn et al., 1989; data not shown). The absence of a strong diagonal in this 2D experiment allows observation of cross-peaks that are otherwise hidden. The ^{15}N chemical shift is unique, and therefore the NH–NH cross-peak to Glu81 could be assigned. This cross-peak between the diagonal positions 8.06 and 7.93 ppm could not be observed in any of the other spectra. Thr80 was assigned completely in the 2D TOCSY spectrum in H_2O. Figure 8 displays a part of the 2D NOE spectrum in H_2O and shows the strong sequential NOEs in the β-sheet region. A schematic representation including NOE connectivities is given in Figure 9. The hydroxyl proton of Tyr73 was assigned in the proton spectrum with a chemical shift of 10.90 ppm. This signal is not present in the ^1H spectrum of the mutant Tyr73Phe-PLA (data not shown). In the 2D NOE spectrum, this proton shows cross-peaks to its aromatic ring protons. In the 1D spectrum of the ^{15}N-labeled PLA this resonance was not doubled, whereas all amide resonances showed clear doublets.

Residues Ser86–Asn88. Ser86 was assigned by using sequential $C_\alpha H$–NH and $C_\beta H$–NH NOEs from Asn85. The NH–NH contact leads to Lys87 with $C_{\beta\beta'}$ positions at 1.79 and 1.42 ppm. For Asn88 the assignment was accomplished on the basis of NH–NH, $C_\alpha H$–NH, and $C_\beta H$–NH connectivities. Asn89 remains unassigned.

α-Helix Ala90–Ala109. A long stretch of sequential NH–NH and $C_\beta H$–NH connectivities was assigned to residues 90–109. In this sequence five alanines are present, which all were completely assigned in the 2D TOCSY spectrum in H_2O. ^{15}N labeling confirmed the assignment for the alanines and

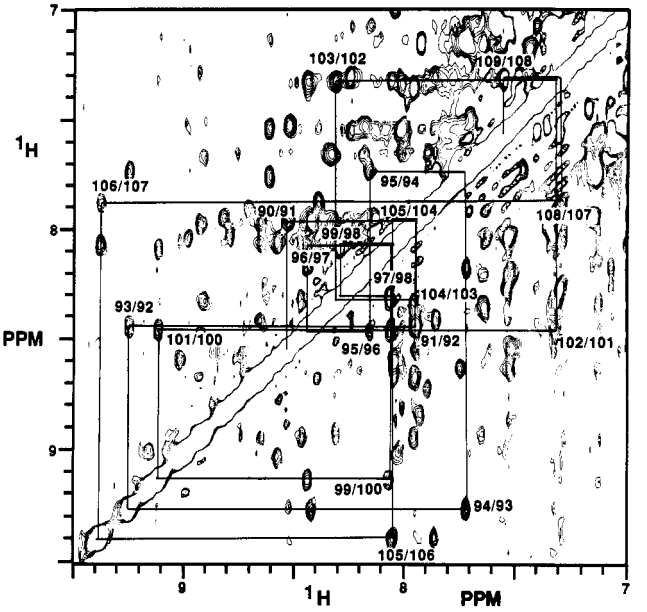

FIGURE 10: Amide region of the 600-MHz 2D NOE spectrum of 1.5 mM PLA (sum of four spectra with mixing times of 25, 50, 100, and 200 ms). The NH–NH connectivities used to establish the α-helix 90–109 are indicated.

yielded specific assignments for Ile95 and Ile104. The sequential assignment for residues Asn97 and Asp99 could not be made with 2D NOESY only, because of overlap of the NH positions of these residues. In the 3D NOESY-HMQC the difference in ^{15}N chemical shift of these two residues overcomes the overlap problem. In Figure 7A the NOE cross-peaks are indicated for residues Phe94, Ala103, and Lys108. In Figure 10 the amide region of the 2D NOE spectrum is shown in which the sequential NH–NH connectivities are indicated for this α-helix. When PLA is freshly dissolved in D_2O, the 2D NOE spectrum shows all the connectivities for residues 93–107 in this α-helix (data not shown).

Residues Pro110–Lys116. The sequential $C_\alpha H$–$C_{\delta\delta'}H$ connectivities from Ala109 and Pro110 were easily assigned, because of the downfield position of the $C_\alpha H$ of Ala109 at 4.79 ppm (Figure 3). The assignment of the amide proton of Tyr111 was based on an NOE to the $C_\alpha H$ of Pro110 and to its ortho ring protons. Sequential $C_\alpha H$–NH NOEs give the assignment of Asn112 and of Lys113. On the basis of strong sequential NH–NH NOEs, residues Lys113, Glu114, His115, and Lys116 could be connected to each other (for the assignment of Lys116 see Figure 7). The His115 amide proton shows a weak NOE to its H4 ring proton. Both Lys113 and Lys116 have TOCSY cross-peaks at 1.99 and 1.96 ppm, respectively, typical for the C_β protons of lysine residues.

Residues Asn117–Cys124. By use of sequential NH–NH, $C_\alpha H$–NH, and $C_\beta H$–NH connectivities, the eight C-terminal residues could be assigned (for residues Asn117, Asp119, Thr120, and Lys121 see Figure 7). The assignment of the amide of Leu118 was confirmed by using the labeling procedure for leucine. The ring protons of Tyr123 have been assigned previously (Fisher et al., 1989), and the assignment of its amide proton is in agreement with this. An NOE between the amide and the ortho ring protons was detected.

The assignments thus far obtained are summarized in Table I. For residues Ile9, Leu41, Tyr52, Phe106, and Tyr111 notable differences in chemical shifts are observed as compared with the results reported by Fisher et al. (1989), but these can be attributed to the slightly higher pH (4.3 instead of 4.1) and lower temperature (313 K instead of 320 K) in our experiments.

Table I: ^{1}H and ^{15}N NMR Resonance Assignments for PLA at 313 K and pH 4.25[a]

residue	^{15}NH	NH	αH	βH	other H
A1			3.87	0.88	
L2	124.7	8.98	4.40	2.01	γ 1.89; $\delta_{1,2}$ 1.12
W3	115.9	8.02	4.48	3.37/3.55	H1 indole 10.40; H2 7.54; H4 7.55; H5 7.31; H6 7.37; H7 7.51
Q4	123.0	6.71	3.90	1.98	
F5	121.6	7.54	4.41	3.31/3.65	o 7.14; m 6.95; p 6.24
R6					γ 1.43/1.89; δ 3.18/3.28; ϵ 7.63
S7	115.1	7.53	4.22	4.22	
M8	124.7	8.61	3.84	2.28	ϵ 1.74
I9	120.8	7.75	3.19	1.66	γ 0.74; γ 0.08, 1.20; δ −0.01
K10	117.7	7.15	3.86	1.92	1.80
C11	117.3	7.66	4.15	3.35/3.46	
A12	118.1	7.66	4.16	1.32	
I13	117.3	8.34	4.36	1.92	γ 0.86, 1.49; δ 0.79
P14			4.63		γ 1.95/2.04; δ 3.52/3.63
G15	109.8	8.70	3.91		
S16	115.1	7.91	4.13	3.80/3.88	
H17	118.1	8.55	5.11	3.12/3.31	H2 8.53; H4 7.36
P18				2.20	γ 1.91; δ 3.63/3.87
L19	119.5	8.54	4.10	1.75	γ 1.75; $\delta_{1,2}$ 0.90
M20	116.8	7.53	4.26	1.92	ϵ 2.00
D21	117.3	8.19			
F22					o 6.78; m, p 7.05
N23					
N24		7.72			
Y25	124.3	7.47	4.56		6.61
G26	114.2	8.13	3.14/3.77		
C27	122.1	11.21	4.78	2.82	
Y28	119.0	11.70			o 7.15; m 6.44
C29	122.5	8.30	5.04	3.55/4.18	
G30	112.9	8.63	4.15		
L31	123.4	8.35	4.37	1.61	γ 1.61; $\delta_{1,2}$ 0.93
G32	112.4	8.29	3.99		
G33	112.4	8.24	3.81/3.98		
S34	118.1	6.65	3.80/4.48		
G35	103.7	8.16	3.83/4.26		
T36	123.0	8.81	4.74	4.07	γ 1.30
P37			4.84	1.90	δ 3.81/3.89
V38	119.5	10.29	3.97	1.67	γ 0.48/0.83
D39	116.8	7.65	4.56	2.90	
E40	118.6	8.63	4.02	2.12/2.21	γ 2.49
L41	125.6	8.78	3.80	1.36	γ 1.06; δ 0.03/0.41
D42	119.9	8.92	5.20	2.93	
R43	120.3	8.34	3.88	1.99/2.09	γ 1.64/1.79; δ 3.26; ϵ 7.36
C44	120.3	8.45	4.48	3.08	
C45	121.6	8.45	4.24	3.59/3.81	
E46	126.0	8.92	3.57	2.08	
T47	117.3	8.63	3.86	4.23	γ 1.20
H48	123.0	7.96	4.45	2.92	H4 6.73
D49	120.8	8.69	4.19	2.94	
N50	120.8	8.39	4.43	2.93	
C51	124.7	8.47	4.47	3.18/3.26	
Y52	119.5	7.97	4.26	2.88/3.25	o 6.68; m 6.20
R53	121.6	7.85	4.05	2.05/2.15	γ 1.67/1.91; δ 3.30; ϵ 7.07
D54	120.8	8.40	4.43	2.79/3.30	
A55	124.3	8.25	3.38	1.52	
K56	113.8	7.32	3.86	1.88	
N57	114.6	7.21	4.68	2.63/2.91	
L58	123.8	7.29	4.18	1.41	γ 1.49; δ 0.42/0.56
D59	127.8	8.91		2.72	
S60	112.0	7.98	4.23	3.77/3.87	
C61	117.3	7.35	4.84	3.11	
K62	122.5	7.96	4.07	1.60	
F63	117.7	8.03	4.60	3.08/3.30	o 7.28; m, p 7.35
L64	121.2	7.67	4.30	1.66	$\delta_{1,2}$ 0.94
V65	118.6	7.91	4.03	2.18	$\gamma_{1,2}$ 0.89
D66	121.2	7.97	4.67	2.71	
N67	117.7	8.09	4.86	2.75/2.95	
P68					γ 1.52; δ 3.60/3.66
Y69	112.9	7.67	4.32	3.03/2.94	o 7.18; m 6.90
T70					
E71					
S72					
Y73	121.2	7.63	4.91	2.66/3.05	o 6.64; m 6.51
S74	115.9	9.72	5.20	3.72	
Y75	130.4	8.88	5.41	3.05/3.15	o 6.97; m 6.65
S76	115.9	8.98	4.38	3.68/3.72	

Table I (Continued)

residue	^{15}NH	NH	αH	βH	other H
C77	122.1	8.66	5.47	3.21/3.04	
S78	123.0	8.82	4.65	3.74/3.78	
N79	126.9	9.37	4.45	2.90/3.09	
T80	110.7	8.06	4.40	4.40	γ 1.19
E81	121.6	7.93	4.58	2.08	γ 2.25/2.32
I82	128.2	8.98	4.77	1.58	γ 1.58; γ 1.01; δ 0.93
T83	124.3	9.14	4.59	3.92	γ 1.08
C84	126.5	9.11	4.65	2.88	
N85	124.3	7.71	4.58	2.53/2.82	
S86	120.8	8.79	4.32	3.97	
K87	119.5	8.02	4.26	1.79	γ 1.42
N88	118.1	7.34	4.72	2.89	
N89					
A90	120.3	8.52	4.11	1.48	
C91	118.1	7.95	4.21	2.79/3.00	
E92	119.0	8.43	3.75	2.18	γ 2.01/2.62
A93	120.3	9.23	3.86	1.42	
F94	122.1	7.71	4.01	3.17/3.30	o 7.07; m 7.54; p 7.41
I95	119.9	8.17	3.32	1.83	0.93, 0.67
C96	120.3	8.43	4.32	2.77	
N97	119.0	8.06	4.25	2.46/2.62	
C98	119.5	8.29	4.33	3.43	
D99	126.9	8.06	3.86	2.76	
R100	124.7	9.10	4.04	1.51/1.81	γ 1.27; δ 2.88/3.17; ε 7.13
N101	115.9	8.44	4.28	2.56/2.76	
A102	123.0	7.33	4.24	0.83	
A103	121.6	8.33	3.33	1.08	
I104	116.4	7.96	3.50	1.73	γ 0.85; 1.08
C105	123.8	8.07	4.20	3.10/3.54	
F106	119.9	9.38	4.28	2.65/3.27	o 6.43; m 6.85; p 7.23
S107	114.2	7.87	4.18	4.01	
K108	121.2	7.31	4.52	1.82	1.58, 2.08
A109	126.0	7.51	4.79	1.36	
P110			4.49		γ 2.09; δ 3.98/3.61
Y111	125.0	8.54	4.23	2.71/3.03	o 6.71; m 6.20
N112	127.8	8.05	5.00	2.42/2.58	
K113	126.5	9.01	3.92	1.99	1.62
E114	118.1	8.70	4.20	1.71	γ 2.25
H115	116.4	8.08	4.45	2.82/2.37	H2 8.76; H4 6.78
K116	121.6	7.02	4.11	1.96	1.58, 1.82
N117	121.6	8.63	4.26	2.75/2.98	
L118	120.3	8.00	4.00	1.20	γ 1.31; δ 0.40/0.44
D119	121.2	8.27	4.72	2.78/3.01	
T120	121.6	8.13	3.91	3.91	γ 1.35
K121	121.6	7.96	4.07	1.81/1.90	γ 1.43
K122	117.7	7.19	4.07	1.23/1.37	γ 0.64/1.05; δ 1.47; ε 2.86
Y123	114.6	7.57	4.60	2.48/3.19	o 7.32; m 6.93
C124	123.0	7.55	4.88	2.87/3.35	

[a] Chemical shifts are reported in ppm relative to the H_2O or HDO signal at 4.60 ppm for ^{1}H and relative to liquid ammonia for ^{15}N.

Exchange Rates. The assignment procedure resulted in an almost completely assigned 2D HMQC spectrum (Figure 6). The 2D HMQC experiment has proven to be suitable to monitor the exchange rates of the amide protons. To this end, the PLA was lyophilized from the H_2O solution, and a 2D HMQC spectrum was recorded in 30 min, directly after the protein (3 mM) was dissolved in D_2O. The exchange was followed by recording a series of 2D HMQC spectra successively (Marion et al., 1989b). Two of the spectra are shown in Figure 11. Panel A is the spectrum recorded directly after the protein was dissolved, while panel B shows the one taken 21.5 h later. The spectrum in panel B contains 28 cross-peaks. Four cross-peaks showed no change in intensity within 21.5 h, and ten cross-peaks showed decay curves characterized by a half-life larger than 43 h, which is twice our experimental time. These amide protons were considered slowly exchanging under our experimental conditions (40 °C and pH 4.3). By comparison with the 2D HMQC spectrum in H_2O (Figure 6) the cross-peaks could be assigned to the amide protons of residues 9–11 and 13 located in the first helix; residues 48–53 located in the second helix; residues 76 and 83 in the β-sheet; residues 93–107 of the third α-helix; and residue 21.

The spectrum in Figure 11A contains 33 cross-peaks, which are absent in the 2D HMQC spectrum recorded 21.5 h after the protein was dissolved and thus represent the amide protons, that show intermediate exchange rates. Among these are the amide protons of residues 3–5, 7–8, and 12 of the first α-helix; 41–47 and 54–58 of the second α-helix; 92 and 108–109 of the third α-helix; and 26 and 81 of the β-sheets. A few decay curves for amides exchanging with the solvent on an intermediate time scale are shown in Figure 12.

The HMQC cross-peaks for Lys10/Lys122, Asn50/Asp54, Leu64/Tyr73, and Glu81/Lys121 were found in the exchange experiment. These cross-peaks are overlapping, and the assignment could not be accomplished by comparison with the reference spectrum (Figure 6) solely. A 2D NOE experiment recorded in D_2O on a sample of unlabeled PLA lyophilized from H_2O was very helpful. In this 2D NOE spectrum the amide protons of Met8–Cys11, His48–Cys51, and Ala93–Ser107 as well as Ser76 and Thr83 were still present and could be assigned on the basis of sequential NOE connectivities. It was clear that the amide protons of Lys10 and Asn50 have half-lives in the range of 5 h or more. The decay curve for the overlapping HMQC cross-peaks of Lys10/Lys122 showed

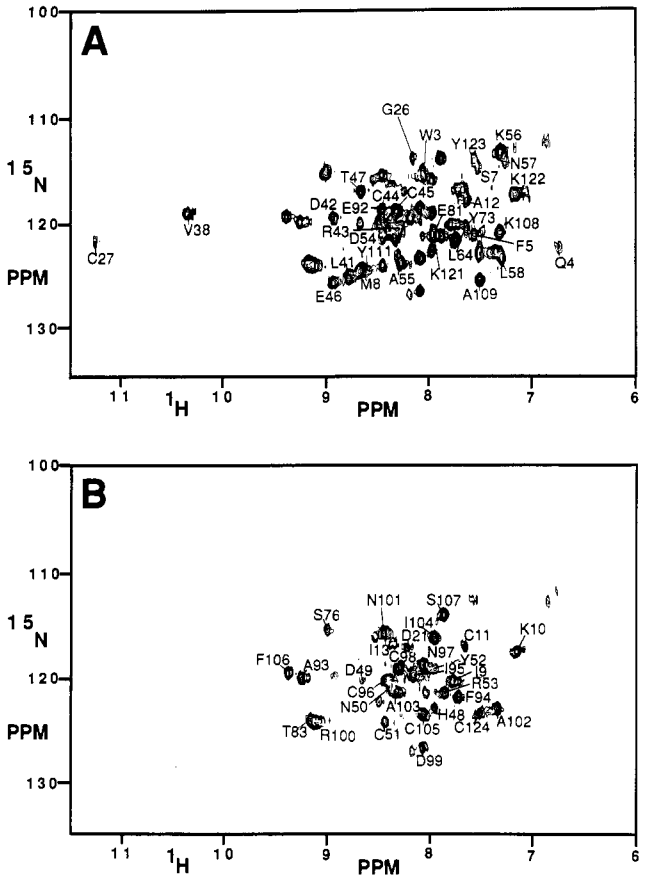

FIGURE 11: 500-MHz ^{15}N–^{1}H HMQC spectrum of 3 mM ^{15}N-labeled PLA, pH 4.3 at 313 K. The protein was freshly dissolved in D_2O after lyophilization from a H_2O solution. (A) Exchange with D_2O for 26 min. (B) Exchange with D_2O for 21.5 h. In (B) all the cross-peaks have been assigned. In (A) those amide protons have been assigned that show an exchange within 20 h.

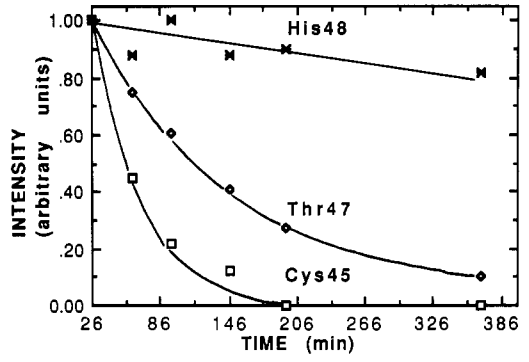

FIGURE 12: Decay curves of the HMQC cross-peak intensities vs time (measured for the recording of the HMQC experiment after dissolving the ^{15}N-labeled PLA in D_2O). Shown are the amide protons exchanging on an intermediate time scale of the second helix of Cys45, Thr47, and His48.

an initial fast decrease but a slower decrease at later times. Since the slow component belongs to Lys10, the fast component must be due to Lys122, and an estimate was made of the half-lives from the beginning and the end of the decay curve separately. The latter assignment was in good agreement with the relatively fast exchange in this C-terminal part. The same behavior was observed for Asn50/Asp54. The slow decay was ascribed to Asn50 and the relatively fast decay to Asp54. Both residues are present in the second α-helix, and the half-lives correspond to the values found for the preceding and following residues. The HMQC cross-peak of Glu81/Lys121 showed an intensity of two protons in the first measurement. The

Table II: Half-Lives for the Amide Exchange in PLA at 313 K and pH 4.25

α-helix 1–13	half-life (h)	α-helix 40–58	half-life (h)	α-helix 90–109	half-life (h)
A1		E40		A90	
L2		L41	1.2	C91	
W3	1.2	D42	<0.5	E92	1.3
Q4	0.6[a]	R43	5[a]	A93	>43
F5	1	C44	1.3[a]	F94	33
R6		C45	<0.5	I95	nm[c]
S7	<0.5	E46	1.6	C96	>43[a]
M8	3.8	T47	2.1	N97	nm
I9	>43	H48	14	C98	>43
K10	23[b]	D49	13	D99	>43
C11	15[a]	N50	7.7[b]	R100	nm[b]
A12	0.8	C51	>43	N101	nm
I13	18[a]	Y52	4.7	A102	>43
		R53	20	A103	20[a]
		D54	1.1[b]	I104	>43
		A55	0.9	C105	>43
		K56	0.5	F106	>43
		N57	<0.5	S107	>43
		L58	<0.5	K108	2.6
				A109	1.8

β-sheet	half-life (h)	others	half-life (h)
G26	<0.5	D21	30[a]
S76	11	C27	0.5
E81	<0.5[b]	Y28	0.5
T83	15	V38	1.1
		L64	0.6[b]
		Y73	0.6[b]
		Y111	11[a]
		K121	<0.5[b]
		K122	0.6[b]
		Y123	<0.5
		C124	>1[a]

[a] Rough estimate, bad fit on data. [b] Overlapping HMQC cross-peak; see text. [c] nm, not measurable; the cross-peak intensity did not decrease more than 10% within 21.5 h.

half-lives could not be obtained separately, but an estimate was made. For the overlap of residues Leu64 and Tyr73 no evidence was present for a specific assignment. In the crystal structure both amide protons form hydrogen bonds.

In total, 61 amide protons show slow or intermediate exchange, 46 of which are located in the three large helices. These amide protons form hydrogen bonds with the corresponding carbonyl groups. Four slowly exchanging protons of residues 26, 76, 81, and 83 are present in a β-sheet. The remaining amide protons are likely to be involved in hydrogen bonds. The half-lives for the exchange with the solvent for the amide protons, which showed slow or intermediate exchange, were calculated by an exponential least-squares analysis and are summarized in Table II.

Dynamics. The central α-helix, 90–109, is very stable. The NH exchange in this part of the structure is characterized by half-lives longer than 43 h for 13 of the protons. In helix 40–58, which flanks the central helix (90–109), the hydrogen-bond network in the center (48–53) is stable, with half-lives in the range of 4.7 to over 43 h, but the ends are more flexible and have half-lives shorter than 5 h.

The low intensity of NOEs involving the backbone protons of the six N-terminal residues is indicative of local mobility in this part of the structure. It is remarkable that this mobility is restricted to the backbone, whereas it is not reflected in the NOEs of the side-chain protons of Trp3 and Phe5.

Different conformations were identified for residue Ser74. The $C_\alpha H$ of this residue was present at two diagonal positions at 5.20 and 5.45 ppm (Figure 3). An exchange cross-peak is present in between these two states. This equilibrium is only found for the $C_\alpha H$. The main conformation is represented by

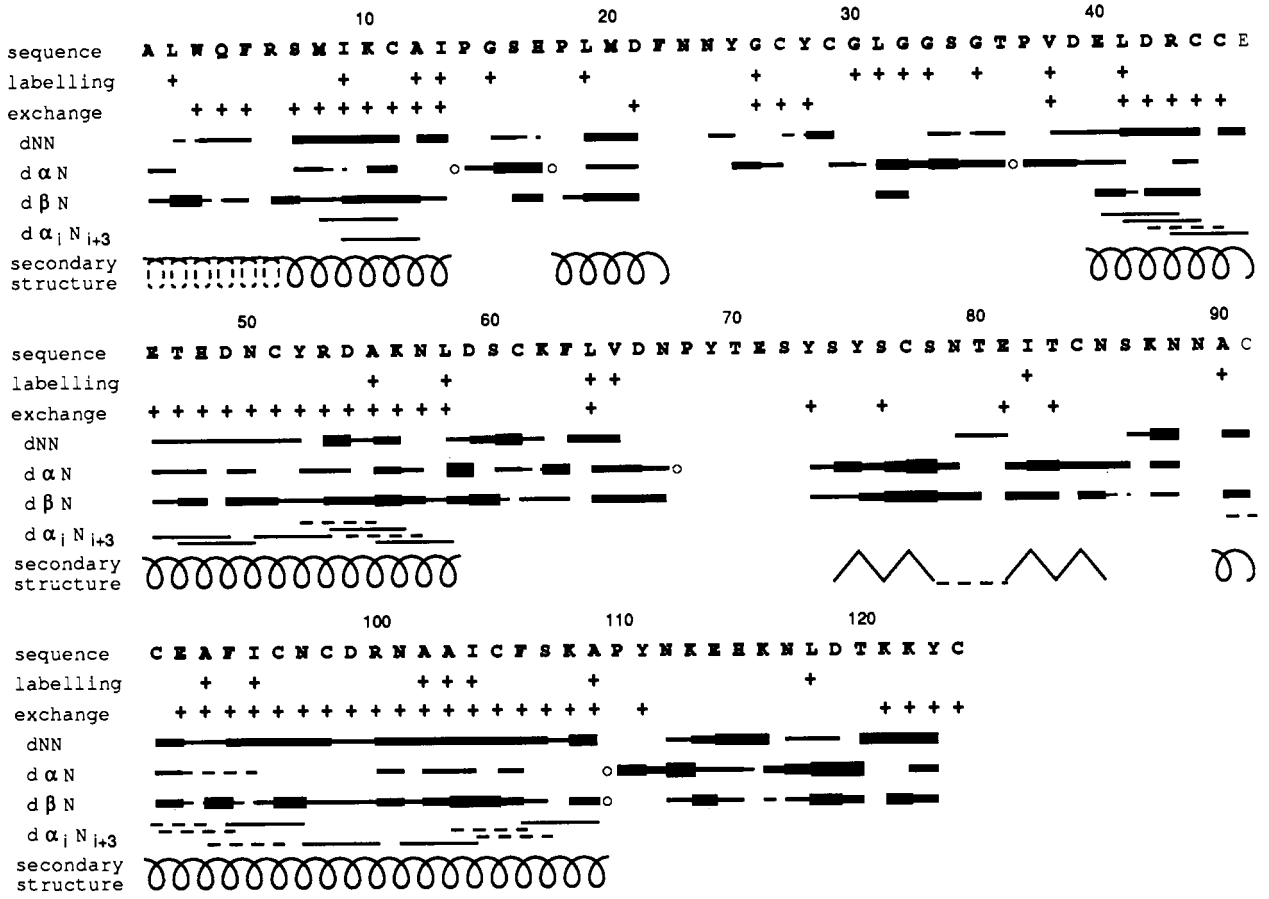

FIGURE 13: Amino acid sequence of PLA with a summary of all short-range NOE connectivities involving the NH, $C_\alpha H$, and $C_\beta H$ protons. The thickness of the bar indicates the observed NOE intensity in the 3D NOESY-HMQC experiment. In a few cases the sequential NOE is only observed in the 2D NOE spectrum, which is indicated by a dashed line. The sequential $C_\alpha H$–$C_{\delta\delta'}H$ connectivity for an X–Pro sequence is indicated by an open circle. The spirals indicate α-helices (dashed for residues 1–6, explained in the text); the jagged line indicates a β-sheet.

the $C_\alpha H$ at 5.20 ppm, which has NOE and TOCSY cross-peaks to the rest of the spin system. The other position shows only connectivities to one of the $C_{\beta\beta'}$ protons in a 2D TOCSY spectrum. It is unlikely that cis–trans isomerization of Pro68 causes this multiplicity of resonances. The equilibrium is also reflected by Tyr73, for which the meta ring protons are broadened to some extent. Local conformational heterogeneity is also indicated for Phe94. An additional resonance position was consistently observed for the ortho ring protons, showing only a weak correlation to the meta ring protons as compared to the main population.

For a number of residues the chemical shift of the amide protons showed large variations in different experiments under very similar conditions. This is apparent especially for Leu2, Leu31, and Leu118. This observation is difficult to interpret.

Secondary Structure: Comparison with Crystal Structures. An overview of the secondary structure as deduced from the NMR data is given in Figure 13. The α-helices are recognized by strong sequential d_{NN} NOEs and by $d_{\alpha N}(i, i + 3)$ NOEs. The latter class of contacts could often not be identified because of overlap with stronger sequential NOEs. Antiparallel β-sheets are recognized by strong sequential $d_{\alpha N}$ NOEs and a parallelogram pattern of contacts as indicated in Figure 9.

The first helix (1–13) is difficult to recognize as such. Apparently it is less stable and less well defined (especially for the first six residues) than in the crystal structure. The helix clearly runs up to Ile13. Helix B (residues 17–22 in the bovine crystal structure) seems to start only at Pro18, which may be due to the difference in the residue at position 17 (glutamine in bovine, histidine in porcine PLA). The backbone protons of Phe22 are unassigned, and therefore the end of the helix is undefined. There is no trace of the hairpin involving residues 25 and 29. These amide protons exchange rapidly, and there is no NOE between them. For helix C (residues 39–58 in the crystal structure), strong sequential d_{NN} NOEs can be seen up to Lys56, but for the next two steps the d_{NN} NOEs are too close to the diagonal. The observation of a $d_{\alpha N}(i, i + 2)$ NOE between residues Ala55 and Asn57 may correspond with the 3_{10} helix as found in the crystal structure. The whole region from Leu58 up to Ser72 seems ill-defined. In the bovine crystal structure, it forms an α-helix and two turns. In the porcine crystal structure, residues Asn67–Glu71 form a 3_{10} helix, and the preceding part is undefined. The NMR data do not indicate a specific secondary structure element for the first part. Residues 70–72 are unassigned. The β-sheet from residues Ser74 to Asn85 is well characterized (see Figures 8 and 9). Remarkably, the amide proton of Ser78 is not hydrogen bonded according to the NH-exchange criterion, while those of Glu81 and Thr83 are. Characteristics of an extended chain are also found for Tyr73 and Ser86. The central helix E (residues 89–108 in the crystal structure) is also very apparent. It extends up to Ala109 in our analysis. At this stage it is not yet clear if the terminal part adopts a 3_{10} conformation. Residues Asn112–Lys116 form two turns, as in the crystal structure. Residues Asp119–Tyr123 show a similar pattern, and this part seems more structured than in the crystal structure of the porcine enzyme. The small antiparallel β-sheet involving residues 24–26 and 115–117 in the crystal structure appears to be present in the solution structure in a shortened form. Only the Gly26 amide proton is hydrogen bonded, and residues Asn24 and Asn117 are not clearly involved.

Concluding Remarks

The sequential assignment confirms (except in the cases noted above) the results of Fisher et al. (1989), who used an assignment procedure based on the crystal structure. In summary, the assignments of the ^{1}H and ^{15}N NMR data were used to establish the secondary structure elements in PLA. We find the secondary structure in solution to be basically the same as in the crystalline state. Differences were found in the following regions, which are less structured in solution: helix 1–6, hairpin 25–29, and β-sheet 24–26 and 115–117. Also, the expected hydrogen bond 78–81 did not show slow exchange behavior.

With the assignments reported in Table I, the residues that form the active center and its surrounding hydrophobic wall have been identified in the 2D spectra. This will allow studies on substrate analogue binding to the enzyme. We have already noted the overlap problem in the 2D NOE spectrum. This seriously hampers obtaining reliable distance constraints from the NOE intensities, but qualitative estimates can be obtained from the better resolved 3D experiment. The present study will form the basis for detailed structure calculations on PLA based on NOE constraints and exchange-rate data, which will allow a more precise definition of the protein structure in solution.

Acknowledgments

We thank Don Dijkstra for his technical assistance with the 3D experiment, Dion Luykx for his preparation of the [^{15}N]leucine- and [^{15}N]glycine-labeled PLA, Bert Verheij for his advice and help in the labeling experiments, Jan den Boesterd for his assistance in preparing the figures, and Jos Joordens and Siebren Wijmenga at the SON hf-NMR facility (Nijmegen University, The Netherlands).

References

Aguiar, A., de Haas, G. H., Jansen, E. H. J. M., Slotboom, A. J., & Williams, R. J. P. (1979) *Eur. J. Biochem. 100*, 511–518.

Bax, A. (1989) *Methods Enzymol. 176*, 151–168.

Bax, A., & Davis, D. G. (1985) *J. Magn. Reson. 65*, 335–366.

Boelens, R., Scheek, R. M., Dijkstra, K., & Kaptein, R. (1985) *J. Magn. Reson. 62*, 378–386.

Braunschweiler, L., & Ernst, R. R. (1983) *J. Magn. Reson. 53*, 521–558.

Brown, S. C., Weber, P. L., & Müller, L. (1988) *J. Magn. Reson. 77*, 166–169.

Brunie, S., Bolin, J., Gewirth, D., & Sigler, P. B. (1985) *J. Biol. Chem. 260*, 9742–9749.

Davis, D. G., & Bax, A. (1985a) *J. Am. Chem. Soc. 107*, 2821–2822.

Davis, D. G., & Bax, A. (1985b) *J. Am. Chem. Soc. 107*, 7198–7199.

de Geus, P., van den Bergh, C. J., Kuipers, O., Verheij, H. M., Hoekstra, W. P. M., & de Haas, G. H. (1987) *Nucleic Acids Res. 15*, 3743–3759.

Dijkstra, B. W., Kalk, K. H., Hol, W. G. J., & Drenth, J. (1981) *J. Mol. Biol. 147*, 97–123.

Dijkstra, B. W., Renetseder, R., Kalk, K. H., Hol, W. G. J., & Drenth, J. (1983) *J. Mol. Biol. 168*, 163–179.

Egmond, M. R., Slotboom, A. J., de Haas, G. H., Dijkstra, K., & Kaptein, R. (1980) *Biochim. Biophys. Acta 623*, 461–466.

Egmond, M. R., Hore, P. J., & Kaptein, R. (1983) *Biochim. Biophys. Acta 744*, 23–27.

Englander, S. W., & Wand, A. J. (1987) *Biochemistry 26*, 5953–5958.

Ernst, R. R., Bodenhausen G., & Wokaun, A. (1987) *Principles of Nuclear Magnetic Resonance in One and Two Dimensions*, Clarendon Press, Oxford.

Fisher, J., Primrose, W. U., Roberts, G. C. K., Dekker, N., Boelens, R., Kaptein, R., & Slotboom, A. J. (1989) *Biochemistry 28*, 5939–5946.

Forst, S., Weiss, J., Elsbach, P., Maraganore, J. M., Reardon, I., & Heinrikson, R. L. (1986) *Biochemistry 25*, 8381.

Griesinger, C., Otting, G., Wüthrich, K., & Ernst, R. R. (1988) *J. Am. Chem. Soc. 110*, 7870–7872.

Gronenborn, A. M., Bax, A., Wingfield, P. T., & Clore, G. M. (1989) *FEBS Lett. 243*, 93–98.

Hayakawa, M., Kudo, I., Tomita, M., Nojima, K., & Inoue, K. (1988) *J. Biochem. (Tokyo) 104*, 767.

Jansen, E. H. J. M., Meyer, H., de Haas, G. H., & Kaptein, R. (1978) *J. Biol. Chem. 253*, 6346–6347.

Jansen, E. H. J. M., van Scharrenburg, G. J. M., Slotboom, A. J., de Haas, G. H., & Kaptein, R. (1979) *J. Am. Chem. Soc. 101*, 7397–7399.

Jeener, J., Meier, B. H., Bachmann, P., & Ernst, R. R. (1979) *J. Chem. Phys. 71*, 4546.

Marion, D., & Wüthrich, K. (1983) *Biochem. Biophys. Res. Commun. 113*, 967–974.

Marion, D., Kay, L. E., Sparks, S. W., Torchia, D. A., & Bax, A. (1989a) *J. Am. Chem. Soc. 111*, 1515–1517.

Marion, D., Ikura, M., Tschudin, R., & Bax, A. (1989b) *J. Magn. Reson. 85*, 393–399.

Müller, L. (1979) *J. Am. Chem. Soc. 101*, 4481.

Nieuwenhuizen, W., Kunze, H., & de Haas, G. H. (1974) *Methods Enzymol. 32B*, 147–154.

Ono, T., Tojo, H., Kuramitsu, S., Kagamiyama, H., & Okamoto, M. (1988) *J. Biol. Chem. 263*, 5732.

Shaka, A. J., Baker, P. B., & Freeman, R. (1985) *J. Magn. Reson. 64*, 547–552.

States, D. J., Haberkorn, R. A., & Ruben, D. J. (1982) *J. Magn. Reson. 48*, 286–297.

Verheij, H. M., Volwerk, J. J., Jansen, E. H. J. M., Puijk, W. C., Dijkstra, B. W., Drenth, J., & de Haas, G. H. (1980) *Biochemistry 19*, 743–750.

Volwerk, J. J., & de Haas, G. H. (1982) in *Lipid Protein Interactions* (Jost, P. C., & Griffith, O. H., Eds.) Wiley, New York.

Waite, M. (1987) *Handbook of Lipid Research: The Phospholipases*, Vol. 5, Plenum, New York.

Wüthrich, K. (1986) *NMR of Proteins and Nucleic Acids*, Wiley, New York.

Zuiderweg, R. P., & Fesik, S. W. (1989) *Biochemistry 28*, 2387–2391.